Variable Ankle Stiffness Improves Balance Control: Experiments on a Bipedal Exoskeleton

Barkan Ugurlu, *Member, IEEE,* Corinne Doppmann, Masashi Hamaya, Paolo Forni, Tatsuya Teramae, Tomoyuki Noda, and Jun Morimoto, *Member, IEEE*

***Abstract*—This paper proposes a real-time balance control technique that can be implemented to bipedal robots (exoskeletons, humanoids) whose ankle joints are powered via variable physical stiffness actuators. To achieve active balancing, an abstracted biped model, torsional spring-loaded flywheel, is utilized to capture approximated angular momentum and physical stiffness, which are of importance in postural balancing. In particular, this model enables us to describe the mathematical relation between Zero Moment Point and physical stiffness. The exploitation of variable physical stiffness leads to the following contributions: i) *Variable physical stiffness* property is embodied in a legged robot control task, for the first time in the literature to the authors' knowledge. ii) Through experimental studies conducted with our bipedal exoskeleton, the advantages of variable physical stiffness strategy are demonstrated with respect to the optimal constant stiffness strategy. The results indicate that the variable stiffness strategy provides more favorable results in terms of external disturbance dissipation, mechanical power reduction, and ZMP/CoM position regulation.**

***Index Terms*—balance control, exoskeleton, variable physical stiffness, ankle stiffness, zero moment point, push recovery.**

I. Introduction

THE advent of the first active exoskeleton reported in [1] led the way to several key developments in the field of lower extremity life support systems. Applications vary from robot-aided physiotherapy [2] and power amplification [3] to walking support for paraplegics [4]–[6] and gait rehabilitation [7]. In [8], Dollar and Herr reviewed a great majority of these devices in terms of design, control, and implementation.

Orienting our research objective within this frame, we developed a high-power, self-balancing, passively compliant and wearable bipedal exoskeleton for robot-aided lower body rehabilitation applications. In particular, the ankle joints of our robot possess the variable physical stiffness feature, which, in turn, effectively allowed the synthesis of a novel balance control strategy to cope with unperceived external disturbances. Therefore, this paper aims to disclose this aspect of our work; the variable physical stiffness property is exploited in the legged robot balancing task for the first time in the literature, to the authors' knowledge.

This study chiefly focuses on the efficacy of the variable physical stiffness modulation to address the legged robot balance control task. The lower body exoskeleton used in our experiments was considered as a bipedal robot without any human user, so as to explicitly examine the sole contribution of the controller. This is due to the fact that humans inadvertently modulate their own muscle impedance characteristics when the human-robot coupled system is perturbed, increasing the complexity of the evaluation. With this in mind, the stability of the human-robot coupled system will be investigated in a future work.

The paper is organized as follows. The current section continues with the discussion on the related works and the contributions presented in this paper. The mechatronic hardware of our bipedal exoskeleton is presented in section II, with a special emphasis on its actuation principle. Variable physical ankle stiffness-based balance recovery control is disclosed in section III with related numeric analyses. Experiment results are discussed in section IV in which a comparison is provided. The paper is concluded in section V by stating the end results and addressing the future direction.

A. Related Works

Incorporation of compliance is of importance for almost all multibody legged systems when considering dependability, intrinsic stability, inherent safety, energy management, and environmental adaptability [9], [10]. In particular, software-controlled active compliance schemes outperformed conventional feedback controllers in handling unperceived environmental conditions and external disturbances [6], [11]–[13]. While this strategy is useful in its own right, it may not be considered inherently safe and energetically favorable due to reflected inertia, high intrinsic impedance, and delays in sensory response and control cycle. [10].

Actuators with elastic components are developed to introduce physical compliance for enhanced human-robot-environment interaction capabilities [14], [15]. On one hand, this actuation principle is effectively used in humanoids and exoskeletons, such as, in balance recovery [16], efficient locomotion [17], and assistive control [18]. On the other hand, physical stiffness characteristics of these actuators are often nonadjustable; thus, enforcing the additional active compliance control schemes to modulate the output impedance. This

The authors are with the Dept. of Brain Robot Interface, Computational Neuroscience Laboratories, Advanced Telecommunications Research Institute International (ATR), 619-0288, Kyoto, Japan. (e-mail: {hamaya, t-teramae, t_noda, xmorimo}@atr.jp)

B. Ugurlu is also with the Dept. of Mechanical Engineering, Ozyegin University, 34794 Istanbul, Turkey. (e-mail: barkan.ugurlu@ozyegin.edu.tr)

C. Doppmann is also with the Dept. of Microengineering, École polytechnique fédérale de Lausanne (EPFL), Lausanne, Switzerland. (e-mail: corinnedoppmann@gmx.ch)

M. Hamaya is also with the Grad. School of Frontier Biosciences, Osaka University, Osaka 565-0871, Japan.

P. Forni is also with the Dept. of Electrical Engineering, Imperial College London, London SW7 2BT, U.K. (e-mail: paolo.forni91@gmail.com)

further requires modulations on the task-specific position or torque inputs in a way so as to emulate the desired impedance characteristics [6], [11], [12], causing inevitable deviations from the position or torque references.

The central nervous system in legged creatures adaptively controls the motion by means of muscle impedance regulation [19]. This allows them to stabilize their motion when subject to disturbances [20], [21], even within the absence of neural feedback [22]. In order to mimic such advanced behavior in robotic systems, researchers developed VIAs (Variable Impedance Actuator) to decouple the apparent output stiffness and actuator torque [23]–[26]. On this matter, VIAs with electrical actuators often require complicated mechanical design, and their implementation to multi-DoF (Degrees of Freedom) systems is an ongoing process due to their size and weight.

Akin to their biological counterparts, PAMs (Pneumatic Artificial Muscle) possess superior characteristics as the main power source. They have great power-to-weight ratios; can drive robot joints without any high-friction mechanical transmission gears. Their implementation to robotic systems is rather simple in terms of mechanical design. More importantly, they act as a simultaneous torque and stiffness generator when antagonistically driven. While PAMs have some disadvantages such as constant need of pressurized air, they were implemented to exoskeleton devices [27]–[29].

Despite the fact that VIAs become increasingly available [26], the *variable physical stiffness* feature has not been thoroughly addressed in legged robot control, particularly, for real-time balance control tasks. There are ongoing efforts in embedding VIAs to legged systems, e.g., [25]; however, a control algorithm that exploits the concept of *variable physical stiffness* has not been proposed in the legged robotics literature. Therefore, the main objective of this paper is to make a contribution in this direction.

B. Novelty

As discussed in [19]–[21], adaptive motion control is provided by means of mechanical impedance regulation in biological muscles. Especially, ankle stiffness modulation is observed to be a key factor in human balancing [21], [30]–[32]. Motivated by the results in these studies, a real-time balance control method is developed for our PAM-powered bipedal exoskeleton which makes use of the *variable physical stiffness* at the ankle joints to cope with unperceived external disturbances.

To extract the mathematical relation between the dynamic balance criterion ZMP (Zero Moment Point) and variable physical stiffness, a torsional spring-loaded flywheel model is constructed by appropriately combining the concepts introduced in [12] and [33] . In doing so, balance control task, i.e., ZMP regulation, can be interpreted in terms of ankle joint stiffness modulation. In addition, the model is able to capture the abstracted angular momentum, which is of importance in postural balancing.

In developing the online balance controller, we offer two contributions:

i) *Variable physical stiffness* property is exploited for the first time in the context of legged robot control, to the authors' knowledge. Software-controlled actively compliant robots [6], [7], [11], [12], and legged systems with nonadjustable physical stiffness [16]–[18] demonstrated favorable locomotion control performances; yet, the utilization of *variable physical stiffness* has not been investigated in the related literature. This paper offers the first implementation of *variable physical stiffness*, with a special emphasis on its efficacy for the real-time balance control of a bipedal system.

ii) The proposed balancing strategy is compared to optimal constant stiffness strategy [16] by conducting experiments on an actual bipedal exoskeleton robot. Results are compared in terms of external disturbance dissipation response, ZMP/CoM (Center of Mass) position regulation, mechanical power reduction, and air mass consumption.

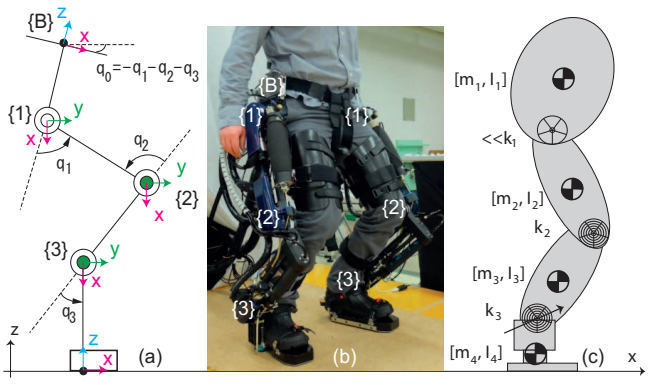

Fig. 1. a) Joint frames of XoR in the sagittal plane. b) The actual robot, XoR, while being worn by an able-bodied. c) Multi-DoF representation of XoR in the sagittal plane. Knee and ankle joints are passively compliant. The arrow on the ankle joint indicates the stiffness variability.

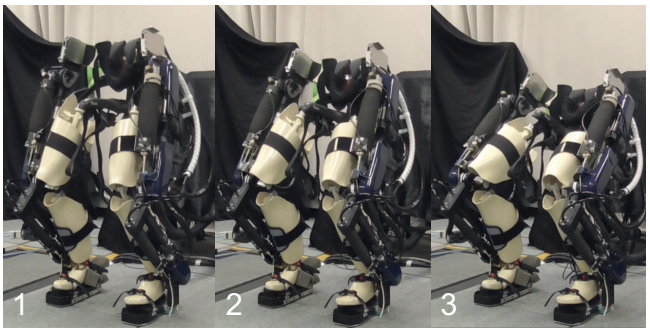

Fig. 2. The PAM-powered exoskeleton robot exhibits its position control functionality by performing self-balanced squatting motion with a dummy mannequin inside [34].

II. A Soft Bipedal Exoskeleton: XoR

In order to conduct research on robot-aided rehabilitation, sensorimotor learning and neurophysiology, a soft bipedal exoskeleton, named XoR, was developed at the BRI - Computational Neuroscience Laboratories of ATR, [29]. Each XoR leg has 3 active DoFs that actuate hip, knee, and ankle joints through flexion/extension. This configuration allows the robot to demonstrate self-balancing and bipedal squatting with no support, nor tethering mechanism; though its motion is

TABLE I
MECHANICAL SPECIFICATIONS OF XOR

Hip - Knee length:	39 [cm]
Knee - Ankle length:	38 [cm]
Ankle - sole length:	14 [cm]
Total Weight	22.2 [kg]

constrained in the sagittal plane. Fig. 1 shows the physical system and its joint frames. Fig. 2 displays three snapshots from the self-balanced squatting experiments with a dummy mannequin. Mechanical specifications of the robot are concisely listed in Table I.

The current version of XoR was chiefly constructed to conduct tasks in the sagittal plane, such as, sit-down and stand-up rehabilitation [2], squatting and active self-balancing. Therefore, this work primarily focuses on planar motions, in which the legs are moved in a synchronized manner. As a consequence, ankle joints are required to output greater torque while hip joints demand the minimum amount of torque output, since no stepping motion is involved in the target tasks.

With this in mind, knee and ankle joints are powered via PAM actuators, due to their high power-to-weight ratio and physical compliance [26]. Ankle joints are driven via two antagonistically coupled PAMs (Festo MAS-10) through flexion/extension, while knee joints are powered via single PAM units (Festo MAS-40) through flexion. Hip joints are actuated via low power motors (Maxon, EC-4 pole). The robot also has hip extensors; however, they are disabled in this study. This hybrid actuation strategy is implemented to comply with the dimensional and weight requirements, in addition to addressing physical compliance and high torque output at the knee and ankle joints.

Ankle joints, powered via antagonistic PAM couples, enables us to control the position (q_3) and the physical stiffness (k_3) in a simultaneous fashion. The details regarding the simultaneous position and variable stiffness control is provided in [34]. Knee joints allow the reliable position control; however, its stiffness (k_2) change depending on the joint state. Utilizing the forward stiffness model and knee torque measurement, we can estimate the changes in k_2 [34]. Hip joints, actuated via low power motors, only enable the position (q_1) control. The stiffness of hip joints is considered sufficiently big, since their physical compliance is relatively insignificant.

In the light of the above stated facts, we model the robot as a 4-link 3-DoF system as displayed in Fig. 1(c), in which ankle joints are driven via variable stiffness actuators, knee joints driven are via passively compliant actuators, and hip joints are driven via stiff-by-nature actuators. Since both legs move in a synchronized manner, the ankle joint stiffness in this model is equivalently distributed to the left and right ankle joints of the robot. This approach was confirmed to be feasible in practice for a passively compliant humanoid [17].

III. BALANCE CONTROL STRATEGY

In order to avoid complex and computationally heavy algorithms, abstracted models with reduced dimensionality are often used in a way so as to capture the important characteristics of multi-body robots for a given task [12], [16], [33]. In line with this strategy, a torsional spring-loaded flywheel model, illustrated in Fig. 3, is utilized to combine the concepts presented in [12] and [33]. In this approach, a flywheel disk with a constant rotational inertia of I_f and a total mass of m is considered to emulate the robot. Flywheel mass is condensed at the robot's CoM position and it is in contact with the floor through a telescopic leg and a rectangular foot. Friction between the foot and the floor is sufficient to prevent foot slips. As the generalized coordinates, leg length r, and angular position with the vertical z-axis, α, are assigned. A torsional spring, with a varying stiffness of k_f, connects the leg to the vertical z-axis. When α=α_0, the spring is in the rest state. The parameter d represents the overall disturbance torque acting on the robot CoM, due to external pushes, and as well as due to modeling uncertainties.

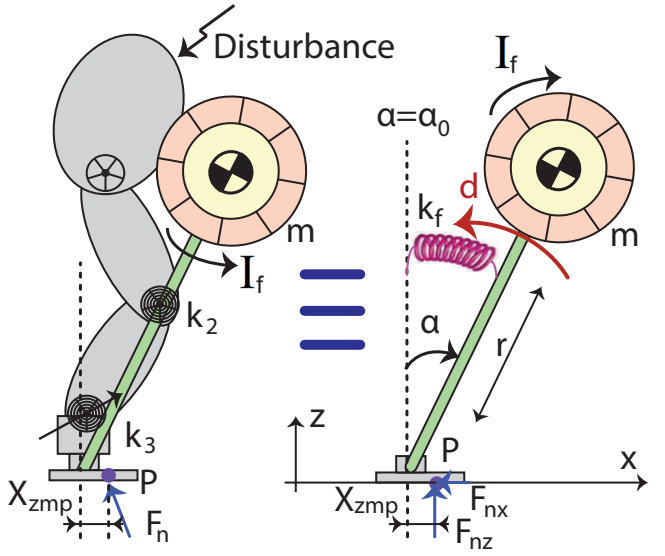

Fig. 3. XoR is modeled as a torsional spring-loaded flywheel pendulum. It can characterize both approximated angular momentum and physical stiffness. Flywheel disk orients in an identical manner with the pendulum. Any disturbance applied on the robot may be represented by d that acts along the α axis. Reaction force F_n can be decomposed to F_{nx} and F_{nz}.

The model offers two beneficial properties. i) Unlike point mass pendulums, it can encapsulate the approximated angular momentum, which is crucial in describing the postural equilibrium. Though the rotational inertia of the robot is joint state dependent (composite rigid body inertia), one can conjecture a constant value by considering the target motion range and CAD data [33]. ii) It can embody the physical stiffness of the robot with the presence of torsional spring. To this end, a mapping between the torsional spring stiffness (k_f) and joint space stiffness (k_2, k_3) will be addressed in the next subsection.

A. Equations of Motion

To derive equations of motion, Lagrangian mechanics is used. r and α are the generalized coordinates.

$$T_{fm} = \frac{1}{2}m\left(\dot{r}^2 + r^2\dot{\alpha}^2\right) + \frac{1}{2}I_f\dot{\alpha}^2 \quad (1)$$

$$U_{fm} = \frac{1}{2}k_f\left(\alpha - \alpha_0\right)^2 + mgr\cos\alpha \quad (2)$$

$$D_{fm} = \frac{1}{2}b_f\dot{\alpha}^2 \quad (3)$$

In these equations, T_{fm} and U_{fm} stand for total kinetic energy and total potential energy. D_{fm} is Rayleigh's dissipation function which is used to embody the frictional and other damping effects through α. The related damping coefficient is b_f. Calculating the Lagrangian of the system via $L_{fm} = T_{fm} - U_{fm}$, the equations of motion can be yielded as follows.

$$\frac{d}{dt}\frac{\partial L_{fm}}{\partial \dot{r}} - \frac{\partial L_{fm}}{\partial r} + \frac{\partial D_{fm}}{\partial \dot{r}} = F_n \quad (4)$$

$$\frac{d}{dt}\frac{\partial L_{fm}}{\partial \dot{\alpha}} - \frac{\partial L_{fm}}{\partial \alpha} + \frac{\partial D_{fm}}{\partial \dot{\alpha}} = M_n \quad (5)$$

Eqs. (4) and (5) respectively stand for translational and rotational motion. F_n and M_n are reaction force and moment acting on the system, see Fig. 3. As described earlier, the friction between the foot and floor is considered to be sufficient to prevent foot slips; therefore, we give our full attention to postural balance which can be described using (5). In this case, reaction moment can be expressed in terms of x-axis ZMP, (X_{zmp}), and vertical reaction force, (F_{nz}) [11].

$$M_n = F_{nz}X_{zmp} + d \quad (6)$$

In (6), d stands for the resultant external moment that may occur due to disturbances. Plugging (6) into (5), the equation of motion is yielded.

$$F_{nz}X_{zmp} + d = (mr^2 + I_f)\ddot{\alpha} + 2mr\dot{r}\dot{\alpha} + k_f(\alpha - \alpha_0) + b_f\dot{\alpha} - mgr\sin\alpha \quad (7)$$

At the right hand side of (7), the rate change of angular momentum that is associated with the rotational inertia is characterized via $I_f\ddot{\alpha}$ term. Physical stiffness is captured with $k_f(\alpha - \alpha_0)$ term.

B. From Flywheel Stiffness to Ankle Stiffness: The Mapping

While (7) reveals the mathematical relation between the ZMP (X_{zmp}) and flywheel stiffness (k_f) in addition to other terms, it is still required to construct a mapping from flywheel stiffness (k_f) to ankle joint stiffness (k_3). To this end, the following equation is used.

$$k_f = (J_{rt}(q)^T)^+ K_r (J_{rt}(q))^+ \quad (8)$$

In (8), the superscript $^+$ stands for the Moore-Penrose pseudo inverse. Recall that the model we use includes only a single torsional spring through α, with a time-varying stiffness parameter k_f; see Fig. 3. There is no translational spring through r. Hence, the stiffness matrix of the model has only one element: k_f. K_r in (8) is a matrix whose diagonal elements store the stiffness values of our robot (k_2, k_3). Note that hip joints do not include physical compliance, thus they are not considered in the mapping as explained in section II. Joint state-dependent $J_{rt}(q)$ is the Jacobian matrix that kinematically maps α to joint coordinates.

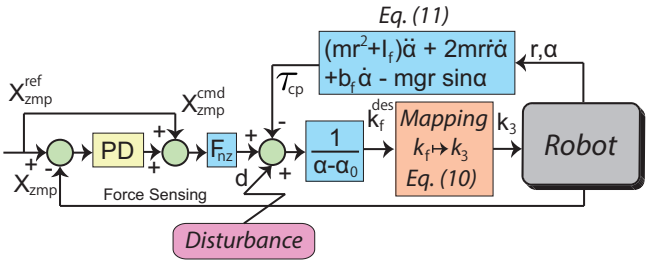

Fig. 4. Our ZMP-based real-time balance controller is based on the variable physical ankle stiffness modulation. Superscripts cmd and ref denote command (controller output) and reference (desired) signals. Position and stiffness control of PAMs [34] is not included in this illustration. The disturbance d represents the resultant external moment that may occur due to any kind of disturbance, e.g., external pushes, modeling uncertainties, etc.

$$J_{rt}(q) = \begin{bmatrix} \frac{\partial \alpha}{\partial q_2} & \frac{\partial \alpha}{\partial q_3} \end{bmatrix} \quad (9)$$

In order to extract the kinematic relation between α and joint coordinates, one can utilize coordinate transformation from polar to Cartesian coordinates and forward kinematics. With (9) at one hand, we can solve (8) to obtain k_3 in terms of k_2 and k_f.

$$k_3 = \frac{k_f\left(J_{rt1}^2 + J_{rt2}^2\right)^2 - k_2 J_{rt1}^2}{J_{rt2}^2} \quad (10)$$

J_{rt1} and J_{rt2} are the first and second elements of $J_{rt}(q)$ and they can be calculated using joint angle measurements. Variations in k_2 can be estimated using the PAM model parameters and torque measurements [34]. Finally, one can obtain k_3 via (10) for a given k_f, together with the estimated k_2, so as to achieve the mapping $k_f \mapsto k_3$.

C. Stable ZMP Feedback Control via Varying Ankle Stiffness

Fig. 4 displays the ZMP feedback control strategy. In order to embody ZMP feedback via the utilization of varying ankle stiffness, we primarily define τ_{cp} which includes the rest of the terms that appear due to inertia, gravity and damping.

$$\tau_{cp} = (mr^2 + I_f)\ddot{\alpha} + 2mr\dot{r}\dot{\alpha} + b_f\dot{\alpha} - mgr\sin\alpha \quad (11)$$

If we compute τ_{cp} using the actual r and α, along with the required time derivatives, and add it up as a compensation block as shown in Fig. 4, we can hypothetically cancel out these terms. On this matter, any modeling and parameter uncertainty would contribute to the disturbance d, which represents the resultant disturbance, including external pushes. Note that actual r and and α can be computed using joint angle measurements. $\ddot{\alpha}$ is obtained with approximate differentiation.

Keeping this in mind, the desired flywheel stiffness, k_f^{des}, is designed as follows, see Fig. 4.

$$k_f^{des} = \frac{F_{nz} X_{zmp}^{cmd} - \tau_{cp}}{\alpha - \alpha_0} \tag{12}$$

Having computed k_f^{des} via (12), we utilize (10) to obtain the corresponding ankle stiffness. The corresponding ankle stiffness is realized in accordance with the simultaneous position and variable stiffness controller that is reported in [34].

In order to prove the stability of the controller disclosed in Fig. 4, we use Lyapunov's theory. First, placing (12) into (7) yields the following.

$$F_{nz} X_{zmp} + d - F_{nz} X_{zmp}^{cmd} = 0 \tag{13}$$

The command signal X_{zmp}^{cmd} is constructed via a PD controller with feedforward, see Fig. 4.

$$X_{zmp}^{cmd} = X_{zmp}^{ref} + K_p e_z + K_d \dot{e}_z \tag{14}$$

Positive PD gains, K_p and K_d, are assigned by respecting the Hurwitz criterion. $e_z = e_z(t)$ is ZMP error; $e_z = X_{zmp}^{ref} - X_{zmp}$. Combining (13) and (14) results as follows.

$$\dot{e}_z = \frac{d}{F_{nz} K_d} - \frac{1 + K_p}{K_d} e_z \tag{15}$$

The Lyapunov function $V(e_z)$ and its time derivative along system trajectories, (15), are derived as below.

$$V(e_z) = \frac{1}{2} \varepsilon e_z^2 \tag{16}$$

$$\dot{V}(e_z) = \varepsilon e_z \dot{e}_z = -\varepsilon \frac{1 + K_p}{K_d} e_z^2 + \varepsilon \frac{d}{F_{nz} K_d} e_z \tag{17}$$

In (16)-(17), ε is a sufficiently small number. Considering the Young's inequality argument, the following condition is met for a sufficiently small coefficient $c_1 > 0$ and a sufficiently large coefficient $c_2 > 0$ [35],

$$\dot{V}(e_z) \leq -c_1 \left\| e_z \right\|^2 + c_2 \left\| \delta(t) \right\|^2, \tag{18}$$

where $\delta(t) = \varepsilon \frac{d}{F_{nz} K_d} e_z$. $\|\cdot\|$ denotes the Euclidean norm. It follows from [36] that the system (13) is Input to State Stable (ISS) with respect to time-varying disturbance $\delta(t)$. This also indicates a notion of robustness for the system (13) through the characterization of the ISS concept. For example, the following expression (definition of ISS) holds true for some $\mathcal{K}$ function Υ and for some $\mathcal{KL}$ function Ω [36].

$$\left\| e_z(t) \right\| \leq \Omega(\left\| e_z(0) \right\|, t) + \Upsilon(\left\| \delta(t) \right\|_\infty) \tag{19}$$

In (19), $\|\cdot\|_\infty$ denotes the infinity norm of the signal $\|\cdot(t)\|$ over time. Intuitively speaking, the definition of ISS requires that for t large, the state must be bounded by some function of the amplitude of the inputs. This to say the norm of the state eventually enters in a ball of radius $\Upsilon(\|\delta(t)\|_\infty)$.

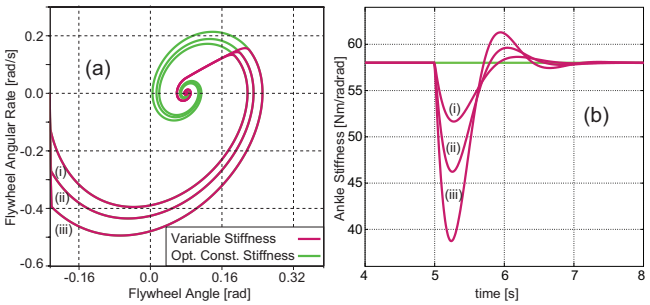

Fig. 5. Numerical simulations were conducted using the torsional spring-loaded flywheel model to compare the proposed and the optimal constant stiffness strategies. 3 distinct external disturbances are implemented to the flywheel CoM. a) Phase diagram, b) Ankle stiffness.

D. Numerical Simulation

In order to observe the differences regarding convergence properties of the proposed balancing strategy with respect to the optimal constant stiffness strategy [16], we ran numerical simulations. In these simulations, disturbances with 3 distinct amplitudes were horizontally implemented to the flywheel CoM for a period of 10 [ms]: i) 50 [N], ii) 100 [N], iii) 150 [N]. Fig. 5 depicts the results in which purple and green lines show phase diagrams and ankle stiffness variations for the proposed balancing strategy and optimal constant stiffness strategy, respectively.

Observing Fig. 5(a), the proposed strategy always converged faster to the equilibrium, compared to the optimal constant stiffness strategy. This was indeed expected, because, when the stiffness was constant, the CoM needed to travel longer to extend the deflection (α-α_0), so as to cope with the disturbance. In contrast, the proposed strategy dynamically modulated the stiffness; therefore, the compensation torque to handle the disturbance could be exerted with comparatively less angular deflection. This allowed the CoM to travel less, resulting in a more favorable balancing strategy as the CoM deviated less from its desired path.

In addition, ankle stiffness appeared to decrease at the time of impact to cope with the disturbance, see Fig. 5(b). It decreased even more when the disturbance amplitude was greater. This was an expected behavior as the disturbance could be dissipated more effectively in higher intrinsic compliance.

IV. Experiment Results

A series experiments were conducted on the bipedal exoskeleton XoR for the proof of concept evaluation. Two experimental protocols were considered: 1) The robot was balanced using the proposed method in which physical ankle stiffness was modulated. This experiment protocol is tagged as VSS. 2) The robot was balanced using the method reported in [16], which allows the computation of the optimal constant ankle stiffness by means of a cost function to optimally minimize ZMP squared. This experiment protocol is tagged as OCS. Using this method, the optimal constant ankle stiffness was calculated as 58 [Nm/rad] for our robot.

The following conditions kept the same in both protocols.
a) The CoM position reference was assigned as a quiet standing state; $r = r_0 = 0.65$ [m] and $\alpha = \alpha_0 = 4.8°$. The method proposed in [34] was used for the position and stiffness control of PAM-powered joints.
b) A pendulum with a tip mass of 4 [kg] and a cable length of 1.25 [m] was released towards the approximate robot CoM by means of an external disturbance source. It was released from an initial angular distance of $15°$ with zero initial velocity. The pendulum tip mass struck the robot when the pendulum angle is approximately $0°$.
c) The pendulum was set free 3 times in a successive manner, with an equal amount of delay in between each hit.
d) Experiments were strictly conducted in 3-D. No tethering, nor supporting mechanism was utilized. The robot also single-handedly bore a bundle of pneumatic and electrical cables attached to its pelvis from the back.

Fig. 6 displays the main results, where solid green and purple lines depict the data collected from OCS and VSS, respectively. Yellow hatched areas indicate the periods in which the pendulum hits the robot to perturb its state, and then the robot reacts to recover from that perturbation.

Horizontal reaction force measurements are provided in Fig. 6(a). This plot shows that the robot motion was disturbed equally in each experiment protocol; see the circled reaction force peaks. The difference is apparent during the recovery stage. The robot was able to dissipate the disturbance when the proposed balancing strategy was used. In the case of VSS, The horizontal reaction force response stayed within the band of ± 24 [N], and settled relatively faster. In contrast, this measurement varied between -50$\sim$75 [N], in the case of OCS.

Fig. 6(b) depicts the physical ankle stiffness variations. As stated previously, the optimal constant ankle stiffness was computed as 58 [Nm/rad] for the case OCS. In the proposed strategy, the ankle joint stiffness was modulated in accordance with the balance control strategy disclosed in section III. When the robot motion was perturbed via the pendulum hits, the ankle stiffness showed a variance between 48$\sim$58 [Nm/rad]. When there was no disturbance, it stayed within the vicinity of the optimal constant stiffness. In order to maintain the balance when disturbed, the higher intrinsic compliance is of importance [10], [25]. By virtue of the decreased ankle stiffness, the disturbance could be effectively dissipated.

ZMP error variations are presented in Fig. 6(c) for the horizontal x-axis. For OCS and VSS, ZMP error varied between -4$\sim$6 [cm] and -1$\sim$2 [cm], respectively. As the proposed method was able to dissipate the external disturbances, ZMP error was well contained for the case of VSS. Compared to the OCS case, peak-to-peak ZMP error was reduced for about 70%. That being said, the robot maintained dynamic balance in both cases, as the ZMP error stayed within the support polygon boundaries.

CoM position error, i.e., flywheel angle deflection plots are given in Fig. 6(d). In the case of OCS, flywheel angle deflection ($\alpha - \alpha_0$) was the only physical quantity that supports the dissipation of the external disturbance. This enforced the CoM to travel more and caused it to deviate from its desired path. In contrast, the proposed balance controller modulated

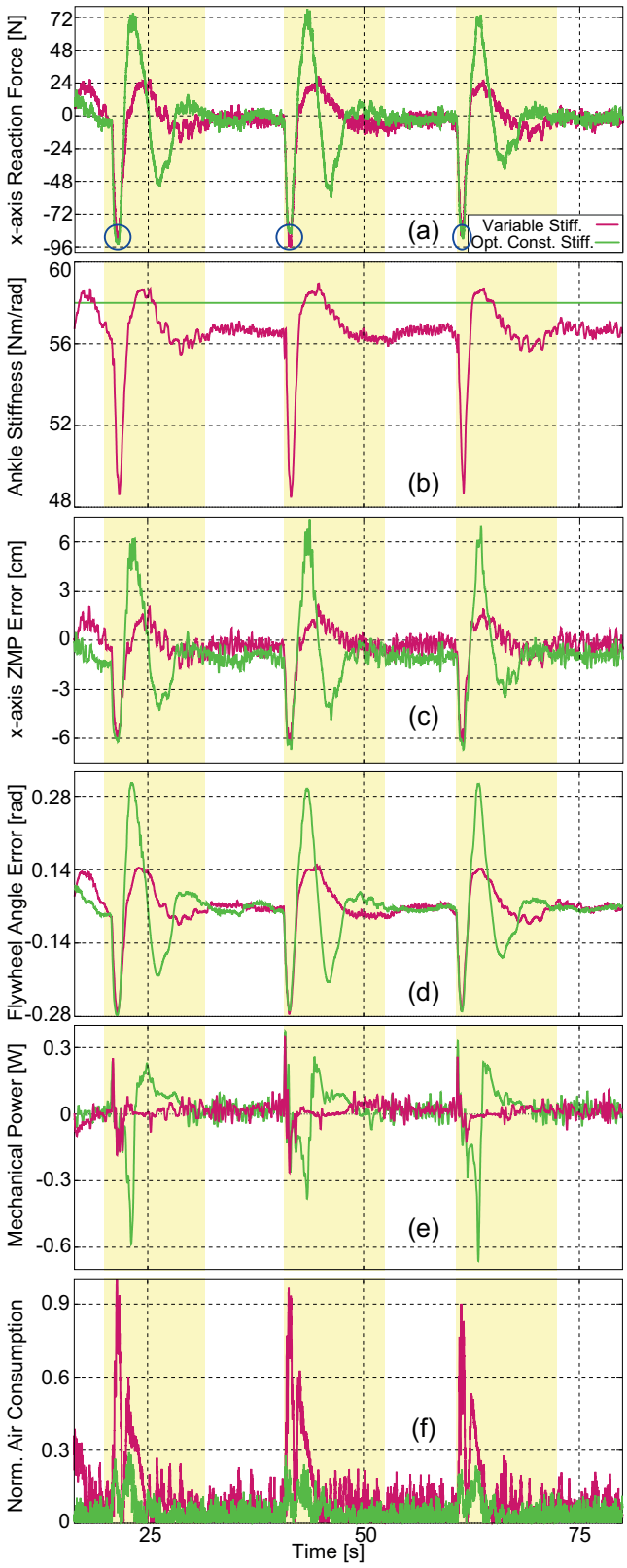

Fig. 6. White areas show delay (rest) periods. Yellow hatched areas indicate the periods in which the robot was hit by the pendulum, and then it reacted to turn back to the quiet standing state. a) Horizontal reaction force measurements. b) Physical ankle stiffness variations. c) ZMP error variations through x-axis. d) Flywheel angular deflections through α axis. e) Total mechanical power plots. f) Normalized air mass consumption plots.

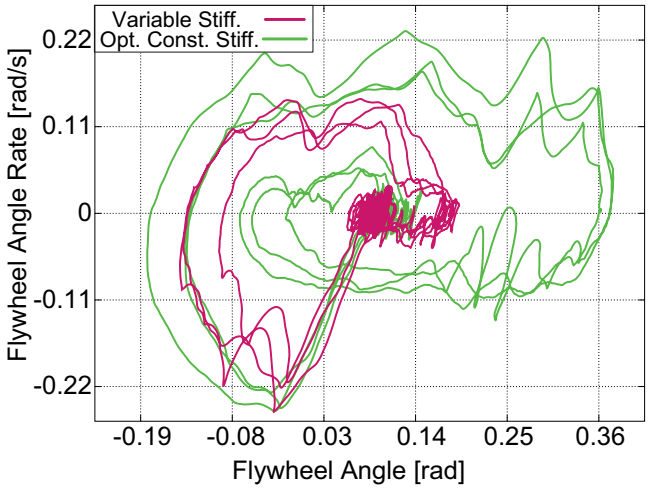

Fig. 7. Phase diagrams through α axis. It is plotted for 3 successive perturbations and the related recovery period. Compared to the OCS case, the CoM converged faster to the quiet standing state when the proposed strategy was employed.

the ankle stiffness in accordance with the ZMP feedback, so as to dissipate the perturbation effectively. As a consequence, CoM position error was contained well as the flywheel angle deflected comparatively less.

Fig. 6(e) depicts the total mechanical power. Since the CoM needed to travel less in the case of VSS, the peak-to-peak mechanical power showed a 50% decrease, compared to the OCS case. Hence, the mechanical power reduction appears to be another advantage of using the proposed method for balancing bipedal systems.

Air mass consumption variations are estimated using ideal gas law and normalized with respect to maximum value; see Fig. 6(f). Examining this figure, the system demanded 70% more air mass in the case of VSS. The main reason behind this increase is that the simultaneous position and stiffness control utilizes the actuator redundancy in the antagonistic architecture, which leads to more aggressive changes in PAM pressure levels. While this negative result should be noted, the increase in supply air is not inherent to this control strategy. We discuss this aspect later in section V.

Fig. 7 illustrates the phase diagrams which were constructed using the experiment data. These phase diagrams indicate that the CoM converged to the equilibrium (quiet standing) much faster in the case of VSS. This result well agrees with numerical simulations presented in Fig. 5. In principle, the proposed balancing strategy modulates the variable ankle stiffness in a way so as to dissipate the external disturbance more effectively, which enables the flywheel angular deflection to be contained more. This helps to decrease CoM position error.

V. Discussion and Concluding Remarks

This paper presented a biologically-inspired novel balance controller that makes use of the *'variable physical'* stiffness for the first time in the legged robot control literature to the authors' knowledge. Through the use of torsional spring-loaded flywheel model, balance recovery via ZMP feedback is addressed by means of physical ankle stiffness modulation. This phenomenon is also observed in humans [21], [30]–[32]. The proposed controller outperformed the optimal constant ankle stiffness strategy in dissipating the external disturbances. This property enabled the robot to exhibit satisfactory balance recovery behavior in terms of convergence rate to the equilibrium state, well-contained ZMP/CoM position error and reduced mechanical power.

That being said, air mass consumption rate appears to increase. While this should be noted as a limitation, this behavior is not inherent to the implemented balance controller. Rather, it is attributed to the nature of antagonistic setups. In [37], Carloni et al. presented a port-based analysis which suggested that a certain portion of power flow is internally stored, and therefore cannot be used to do work, during the nominal operation of variable stiffness actuators with antagonistic setups. Since PAMs must be antagonistically coupled to generate bidirectional joint torque, increased air mass consumption rate is inevitable, in particular, when the stiffness is modulated.

Numerical simulations also showed that the proposed method outperforms the optimal constant ankle stiffness method. After disturbing three times with different amplitudes, the CoM travels less when returning to the equilibrium position in each case. This is in good agreement with the experiment results. Moreover Fig. 6(a) indicates that the horizontal impact was around 100 [N] in our experiments. This caused a drop in ankle stiffness up to 48.5 [Nm/rad]. A comparable drop is also seen in the second numeric simulation; implementing a perturbation of 100 [N] led to a decrease in ankle joint up to 46.5 [Nm/rad].

The proposed controller utilizes the ankle joint. In [38], Stephen showed that hip strategy could be utilized in addition to ankle strategy. While the proposed method can be accordingly enhanced for a robot with variable stiffness hip joints, ankle strategy was observed to be the main and primary stabilization action in humans [39]. The study in [39] also emphasized that no 'hip-only' strategy was observed; rather, it appears to be an auxiliary stabilization action to support the ankle strategy. With this in mind, this study focused on the so-called ankle strategy. Currently, our bipedal exoskeleton XoR is under hardware maintenance to provide variable stiffness in all joints. Upon the completion of this modification, auxiliary supportive strategies will be investigated on top of the proposed controller.

Speaking of auxiliary controllers, Morasso and Sanguineti defended that ankle stiffness modulation alone is not sufficient to stabilize human quiet standing [40]. Indeed this is expected, as the achievable stiffness range has upper and lower bounds for biological muscles. Akin to their biological counterparts, PAM-powered joints have certain stiffness operation ranges as well. Depending on the disturbance amplitude, the desired ankle stiffness may be out of the operation range, potentially hampering the success of the stabilization. Since this is a certain limitation for almost all the muscle-powered systems, one may utilize additional strategies when the stiffness saturation occurs. Another possible solution is to use variable stiffness actuators with theoretically infinite stiffness range, such as the

one reported in [23], although such actuators have not been fully downsized yet to power multi-DoF systems. Therefore, the maximum disturbance that can be handled by the controller is hardware-dependent.

After the hardware modification on XoR, the future work will include the development of the auxiliary strategies, on top of the proposed baseline stabilizer that utilizes physical ankle stiffness. In addition, human-robot coupled stability will be scrutinized to eventually address real-time balance control while the robot is utilized in clinical rehabilitation tests.

ACKNOWLEDGEMENTS

This research was supported by SRPBS of the MEXT, the New Energy and Industrial Technology Development Organization (NEDO), ImPACT Program of Council for Science, Technology and Innovation (Cabinet Office, Government of Japan), the contract with the Ministry of Internal Affairs and Communications entitled 'Novel and innovative R&D making use of brain structures', MEXT KAKENHI 23120004, JSPS KAKENHI 24700203 and 15H05321, JST-SICP, MIC-SCOPE, and JSPS-MIZS: Japan-Slovenia Research Co- operative Program. The authors thank A. Inano, N. Nakano, and G. Lisi for their kind assistance.

REFERENCES

[1] M. Vukobratovic, D. Hristic, and Z. Stojiljkovic, "Development of active anthropomorphic exoskeletons," in *Medical and Biological Engineering*, vol. 12, no. 1, 1974, pp. 66-80.

[2] A. Tsukahara, R. Kawanishi, Y. Hasegawa, and Y. Sankai, "Sit-to-stand and stand-to-sit transfer support for complete paraplegic patients with robot suit HAL," in *Advanced Robotics*, vol. 24. no. 11, 2010, pp. 1615-1638.

[3] H. Kazerooni, "Human augmentation and exoskeleton systems in Berkeley," in *Int. Journal of Humanoid Robotics*, vol. 4, no. 3, 2007, pp. 575-605.

[4] P. D. Neuhaus, J. H. Noorden, T. J. Craig, T. Torres, J. Kirschbaum and J. E. Pratt, "Design and evaluation of Mina, a robotic orthosis for paraplegics," in *Proc. IEEE Conf. on Rehabilitation Robotics*, Zurich, Switzerland, 2011, pp. 1-8.

[5] A. Esquenazi, M. Talaty, A. Packel, M. Saulino, "The ReWalk powered exoskeleton to restore ambulatory function to individuals with thoracic-level motor-complete spinal cord injury," in *American Journal of Phys. Med. Rehabil.*, vol. 91, no. 11, 2012, pp. 911-921.

[6] B. Ugurlu, H. Oshima, and T. Narikiyo, "Lower body exoskeleton-supported compliant bipedal walking for paraplegics: How to reduce upper body effort?" in *Proc. IEEE Conf. on Robotics and Automation*, Hong Kong, China, 2014, pp. 1354- 1360.

[7] J. F. Veneman, R. Kruidhof, E. E. G. Hekman, R. Ekkelenkamp, E. H. F. Van Asseldonk, and H. van der Kooij, "Design and evaluation of LOPES exoskeleton robot for interactive gait rehabilitation," in *IEEE Trans. on Neural Systems and Rehabilitation Engineering*, vol. 15, no. 3, 2007, pp. 379-386.

[8] A. M. Dollar, and H. Herr, "Lower extremity exoskeletons and active orthoses: Challenges and state-of-the-art," in *IEEE Trans. on Robotics*, vol. 24, no. 1, 2008, pp. 144-158.

[9] A. De Santis, B. Siciliano, A. De Luca, and A. Bicchi, "An atlas of physical human-robot interaction," in *Mechanism and Machine Theory*, vol. 43, no. 3, 2008, pp. 253-270.

[10] M. Zinn, O. Khatib, B. Roth, and J. K. Salisbury, "Playing it safe [human-friendly robot]," in *IEEE Robotics & Automation Magazine*, vol. 11, no. 2, 2004, pp. 12-21.

[11] S.-H. Hyon, "Compliant terrain adaptation for biped humanoids without measuring ground surface and contact forces," in *IEEE Trans. on Robotics*, vol. 25, no. 1, 2009, pp. 677-688.

[12] J.-Y. Kim, I.-W. Park, and J.-H. Oh, "Experimental realization of dynamic walking of the biped humanoid robot KHR-2 using zero moment point feedback and inertial measurement," in *Advanced Robotics*, vol. 20, no. 6, 2006, pp. 707-736.

[13] H. Woo, and K. Kong, "Controller design for mechanical impedance reduction", in *IEEE Trans. on Mechatronics*, vol. 20, no.2, 2014, pp. 845-854.

[14] G. A. Pratt, P. Willisson, C. Bolton, and A. Hofman "Late motor processing in low-impedance robots: impedance control of series-elastic actuators," in *Proc. IEEE Conf. on American Control Conference*, Boston, US, 2004, pp. 3245-3251.

[15] A. Girard, J.-P. L. Bigue, B. M. O'Brien, T. A. Gisby, I. A. Anderson, and J.S. Plante, "Soft two-degree-of-freedom dielectric elastomer position sensor exhibiting linear behavior", in *IEEE Trans. on Mechatronics*, vol. 20, no. 1, 2014, pp. 105-114.

[16] M. Mosadeghzad, N. G. Tsagarakis, G. A. Medrano-Cerda, and D. G. Caldwell, "Power efficient balancing control for humanoids based on approximate optimal ankle compliance regulation," in *Proc. IEEE Conf. on Robotics and Automation*, Hong Kong, China, 2014, pp. 5103-5108.

[17] B. Ugurlu, J. A. Saglia, N. G. Tsagarakis, S. Morfey, and D. G. Caldwell, "Bipedal hopping pattern generation for passively compliant humanoids: Exploiting the resonance," in *IEEE Trans. on Industrial Electronics*, vol. 61, no. 10, 2014, pp. 5431-5443.

[18] N. C. Karavas, A. Ajoudani, N. Tsagarakis, J. Saglia, A. Bicchi, and D. G. Galdwell, "Tele-impedance based assistive control for a compliant knee exoskeleton," in *Robotics and Autonomous Systems*, in press.

[19] N. Hogan, "Adaptive control of mechanical impedance by coactivation of antagonist muscles," in *IEEE Trans. on Automatic Control*, vol. 29, no. 8, 1985, pp. 681-690.

[20] E. Burdet, R. Osu, D. Franklin, T. E. Milner, and M. Kawato, "The central nervous system stabilizes unstable dynamics by learning optimal impedance," in *Nature*, vol. 414, 2001, pp. 446-449.

[21] C. Y. Ho, and A. P. Bendrups, "Ankle reflex stiffness during unperceived perturbation of standing in elderly subjects" *The journals of gerontology. Series A, Biological sciences and medical sciences*, vol. 57, no. 9, 2002, pp. 344-350.

[22] E. Taub, P. Perrella, and G. Barro, "Behavioral development after forelimb deafferentiation on day of birth in monkeys with and without blinding", in *Science*, vol. 181, no. 4103, 1973, pp. 959-960.

[23] A. Jafari, N. G. Tsagarakis, I. Sardellitti, and D. G. Caldwell, "A new actuator with adjustable stiffness based on a variable ratio lever mechanism", in *IEEE Trans. on Mechatronics*, vol. 19, no. 1, 2014, pp. 55-63.

[24] G. Mathijssen, D. Lefeber, and B. Vanderborght, "Variable recruitment of parallel elastic elements: Series-parallel elastic actuators (SPEA) with dephased mutilated gears", in *IEEE Trans. on Mechatronics*, vol. 20, no. 2, 2014, pp. 594-602.

[25] H. Yu, S. Huang, G. Chen, and N. Thankor, "Control design of a novel compliant actuator for rehabilitation robots," in *Mechatronics*, vol. 23, no. 8, 2013, pp. 1072-1083.

[26] B. Vanderborght, A. Albu-Schaeffer, A. Bicchi, E. Burdet, D. G. Caldwell, R. Carloni, M. Catalano, O. Eiberger, W. Friedl, G. Ganesh, M. Garabini, M. Grebenstein, G. Grioli, S. Haddadin, H. Hoppner, A. Jafari, M. Laffranchi, D. Lefeber, F. Petit, S. Stramigioli, N. Tsagarakis, M. Van Damme, R. Van Ham, L. C. Visser, and S. Wolf, "Variable impedance actuators: A review," in *Robotics and Autonomous Systems*, vol. 61, no. 12, 2013, pp. 1601-1614.7

[27] N. G. Tsagarakis, and D. G. Caldwell, "Development and control of a 'soft-actuated' exoskeleton for use in physiotherapy and training," in *Autonomous Robots*, vol. 15, no. 1, 2003, pp. 21-33.

[28] P. Beyl, M. Van Damme, R. Van Ham, B. Vanderborght, and D. Lefeber, "Pleated pneumatic artificial muscle-based actuator system as a torque source for compliant lower limb exoskeleton", in *IEEE Trans. on Mechatronics*, vol. 19, no. 3, 2014, pp. 1046-1056.

[29] S.-H. Hyon, J. Morimoto, T. Matsubara, T. Noda, and M. Kawato, "XoR: Hybrid drive exoskeleton robot that can balance," in *Proc. IEEE Conf. on Intelligent Robots and Systems*, San Francisco, US, 2011, pp. 2715-2722.

[30] D. Engelhart, A. C. Schouten, R.G.K.M. Aarts, and H. van der Kooij, "Assessment of multi-joint coordination and adaptation in standing balance: a novel device and system identification technique" *IEEE Trans. on Neural Systems and Rehabilitation Engineering*, in press.

[31] R. C. Fitzpatrick, J. L. Taylor, and D. I. McCloskey, "Ankle stiffness of standing humans in response to imperceptible perturbation: Reflex and task-dependent components," in *Journal of Physiology*, vol. 454, 1992, pp. 533-547.

[32] D. A. Winter, F. Prince, P. Stergiou, and C. Powell, "Medial-lateral and anterior-posterior motor responses associated with centre of pressure changes in quiet standing," in *Neuroscience Research Communications*, vol. 12, no. 3, 1999, pp. 161-170.

[33] J. Pratt, J. Carff, S. Drakunov, and A. Goswami, "Capture point: A step toward humanoid push recovery," in *Proc. IEEE Conf. on Humanoid Robotics*, Genova, Italy, 2006, pp. 200-207.
[34] B. Ugurlu, P. Forni, C. Doppmann, and J. Morimoto, "Stable Control Modes for Pneumatic Muscle Actuators: Force, Position and Variable Stiffness," under review.
[35] D. Angeli, E. Sontag, and Y. Wang, "A characterization of integral input-to-state stability," in *IEEE Trans. on Automatic Control*, vol. 45, no. 26, 2000, pp. 10821097.
[36] E. Sontag, "Input to state stability: Basic concepts and results," in *Nonlinear and Optimal Control Theory, Lecture Notes in Mathematics*, Springer, 2004, pp. 163220.
[37] R. Carloni, L. C. Visser, and S. Stramigioli, "Variable stiffness actuators: A port-based power-flow analysis," in *IEEE Trans. on Robotics*, vol. 28, no. 1, 2012, pp. 1-11.
[38] B. Stephens, "Integral control of humanoid balance," in *Proc. IEEE Conf. on Intelligent Robots and Systems*, San Diego, US, 2007, pp. 4020-4027
[39] C. F. Runge, C. L. Shupert, F. B. Horak, and F. E. Zajac, "Ankle and hip postural strategies defined by joint torques," in *Gait & Posture*, vol. 10, no. 2, 1999, pp. 161-170.
[40] P. G. Morasso, and V. Sanguineti, "Ankle stiffness alone cannot stabilize balance during quiet standing," in *Journal of Neurophysiology*, vol. 88, no. 4, 2002, pp. 2157-2162.

Barkan Ugurlu (S'08-M'10) received his Ph.D. degree in Electrical and Computer Engineering from Yokohama National University, Yokohama, Japan, in March 2010. From May 2010 to March 2013, he was a Post-Doctoral Researcher, at the Istituto Italiano di Tecnologia, Genova, Italy, and Toyota Technological Institute, Nagoya, Japan. Between March 2013 and February 2015, he was a Research Scientist at the Computational Neuroscience Laboratories, Advanced Telecommunications Research Institute International (ATR), Kyoto, Japan. He currently holds an Assistant Professor position at the Dept. of Mechanical Engineering, Ozyegin University, Istanbul, Turkey. His research interests include biological sensorimotor control and motor recovery, active orthoses and exoskeletons, robot-aided rehabilitation, and humanoid/quadruped locomotion control.

Corinne Doppmann received her B.Sc. and M.Sc. degrees in Microengineering from the École polytechnique fédérale de Lausanne (EPFL), Switzerland. In 2014, she was an intern student working on her Master Thesis on exoskeleton robots at the Computational Neuroscience Laboratories, Advanced Telecommunications Research Institute International (ATR), Kyoto, Japan. Since then, she has been with National Instruments Switzerland GmbH, Ennetbaden, Switzerland, where she is currently working as an Applications Engineer.

Masashi Hamaya received his B.E. degree from Kobe University, Kobe, Japan, in 2013. He is currently working toward the M.S. degree in the Graduate School of Frontier Biosciences, Osaka University, Osaka, Japan. He is also currently with the Department of Brain Robot Interface, ATR Computational Neuroscience Laboratories, Kyoto, Japan. His research interests include active exoskeleton robots and optimal control.

Paolo Forni received his B.S.E. in Computer Science and Control Engineering from the University of Rome, Italy, in 2012, and the M.Sc. in Control Engineering from Delft University of Technology, The Netherlands, in 2014. He is currently pursuing the Ph.D. degree in the Control and Power group in Imperial College, London, U.K. His main research interests are in stability of nonlinear dynamical systems, and control of port-Hamiltonian systems.

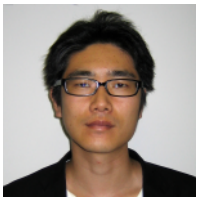

Tatsuya Teramae received his Ph.D. in Engineering from Tottori University, Japan, in 2011. He is currently a researcher at the Department of Brain Robot Interface, ATR Computational Neuroscience Laboratories, Kyoto, Japan. His research interests include optimal control and human machine interfaces. He is a member of the Society of Instrument and Control Engineers, Japan, and the Institute of Electrical Engineers of Japan.

Tomoyuki Noda received his Ph.D. degree in Engineering from the Graduate School of Osaka University, Osaka, Japan, in 2009. He then joined the Institute for Neural Computation in University California San Diego as a visiting Research Scholar. In 2010, he started to work as a Post-Doctoral Researcher at the Computational Neuroscience Laboratories of ATR, Kyoto, Japan. Dr. Noda was nominated for the Best Video Award at IEEE AAAI 2008, and is the recipient of the Best Video Award in LAB-RS 2008, regarding the development of a whole body humanoid robot with tactile sensation and compliant joints. He was nominated for the Best Paper Award at IEEE Humanoids2012 with his work on a BMI-controlled exoskeleton.

Jun Morimoto (M'08) received the Ph.D. degree in Information Science from the Nara Institute of Science and Technology, Nara, Japan, in 2001. From 2001 to 2002, he was a postdoctoral fellow at the Robotics Institute, Carnegie Mellon University, Pittsburgh, PA, USA. Since 2002, he has been at the Advanced Telecommunications Research Institute International, Kyoto, Japan, where he was a Researcher in the Computational Brain Project, the International Cooperative Research Project, Japan Science and Technology Agency from 2004 to 2009. He is currently the head of the Department of the Brain Robot Interface, ATR Computational Neuroscience Laboratories, Kyoto, Japan.